Electronic Supplementary Information (ESI)

Dual-response fluorescence sensing toward $H_2PO_4^-$ and CO_3^{2-} by AJP filter paper based on a pH-stable Cd^{II}-based luminescent metal-organic framework

Xiao-Qin Cao,[a]‡ Qiang Li,[a]‡ Shu-Li Yao,[c] Li-qin Zhong,[d] Lei Cao,[d] Yong-Qiang Chen[b]* and Sui-Jun Liu[a]*

[a]School of Chemistry and Chemical Engineering, Jiangxi Provincial Key Laboratory of Functional Molecular Materials Chemistry, Jiangxi University of Science and Technology, Ganzhou 341000, Jiangxi Province, P.R. China.

[b]Department of Chemistry and Chemical Engineering, Jinzhong University, Jinzhong 030619, Shanxi Province, P.R. China.

[c]School of Rare Earth and New Materials Engineering, Ganzhou Key Laboratory of Advanced Processing and Technology Optimization of High Performance Tungsten Base Materials, Gannan University of Science and Technology, Ganzhou 341000, Jiangxi Province, P.R. China.

[d]Laboratory of Advanced Materials & Manufacturing (LAMM), Jiangxi Provincial Key Laboratory for Simulation and Modelling of Particulate Systems, Jiangxi University of Science and Technology, Nanchang 330013, P.R. China.

*Corresponding authors. E-mail: sjliu@jxust.edu.cn (S.-J. Liu), chenjzxy@126.com (Y.-Q. Chen)

‡These authors contributed equally to this work and should be considered co-first authors.

Materials and methods

BIBT was synthesized according to the reported literature by our group.[S1] Other reagents and solvents were purchased from commercial sources and used without further purification. IR spectra were measured on a Bruker ALPHA FT-IR spectrometer. Thermogravi-metric analyses (TGA) were performed on a NETZSCH STA2500 (TG/DTA) thermal analyzer under a nitrogen flow. Powder X-ray diffraction (PXRD) patterns were documented with Rigaku Miniflex 600. UV/vis absorptions spectra for all samples were measured with a UV-2500 spectrophotometer. Fluorescence measurements were carried out on an F4600 (Hitachi) fluorescence spectrophotometer. The luminescence lifetimes were recorded on a HORIBA Fluorolog fluorescence spectrophotometer. A commercial AJP printer (HMP, WE Electronics, China) was used for AJP **JXUST-32** ink.

Table S1. Crystal data and structure refinements for **JXUST-32**.

Complex	**JXUST-32**
formula	$C_{24}H_{14}CdN_6O_4S$
M_r	594.87
T (K)	293
crystal system	Triclinic
space group	$P\bar{1}$
a (Å)	9.2405(4)
b (Å)	10.3715(4)
c (Å)	13.1210(5)
α (º)	105.957(1)
β (º)	100.975(1)
γ (º)	93.323(1)
V (Å^3)	1178.79(8)
Z	2
F(000)	592.0
D_{calc} (g cm^{-3})	1.676
μ (mm^{-1})	1.06
Reflections collected/unique	18154/5406
R_{int}	0.090
$R_1{}^a$/w$R_2{}^b$ [I>2σ(I)]	0.0890/0.2170
$R_1{}^a$/w$R_2{}^b$ (all data)	0.1173/0.2348
GOF on F^2	1.097

$^aR_1 = \Sigma(||F_0| - |F_C||)/\Sigma|F_0|$. $^bwR_2 = [\Sigma w(|F_0|^2 - |F_C|^2)^2/(\Sigma w|F_0|^2)^2]^{1/2}$.

Table S2. Selected bond lengths (Å) and angles (°) for **JXUST-32**.

Cd1—O1	2.510(8)	Cd1—O4	2.390(7)
Cd1—O2	2.250(7)	Cd1—N1	2.277(8)
Cd1—O3	2.311(6)	Cd1—N6^{i}	2.271(7)
O3—Cd1^{iii}	2.418(3)		
O2—Cd1—O1	54.2(2)	N1—Cd1—O1	141.7(3)
O2—Cd1—O3	142.0(3)	N1—Cd1—O3	119.2(3)
O2—Cd1—O4	97.2(3)	N1—Cd1—O4	97.9(3)
O2—Cd1—N1	87.5(3)	N6^{i}—Cd1—O1	93.0(3)
O2—Cd1—N6^{i}	112.2(3)	N6^{i}—Cd1—O3	89.0(3)
O3—Cd1—O1	95.3(3)	N6^{i}—Cd1—O4	144.3(3)
O3—Cd1—O4	55.4(2)	N6^{i}—Cd1—N1	103.0(3)
O4—Cd1—O1	88.0(3)		

Symmetry codes: (i) x+1, y+1, z; (ii) -x, -y+2, -z+2; (iii) -x+2, -y+1, -z+2;

Table S3. SHAPE analysis of the Cd^{II} ion in **JXUST-32**.

ion	**label**	**shape**	**symme**	**distortion(τ)**
Cd1	HP-6	Heptagon	D_{6h}	34.078
	PPY-6	Pentagonal pyramid	C_{5v}	18.954
	OC-6	Octahedron	O_h	**8.617**
	TPR-6	Trigonal prism	D_{3h}	**9.485**
	JPPY-6	Johnson pentagonal pyramid J2	C_{5v}	23.685

Table S4. Comparison of different MOF materials for detecting $H_2PO_4^-$.

Sensors	**Detection technique**	**Limit of detection (LOD)**	**Refences**
F-MOF	turn-off fluorescence	3.903 μM	S2
$[Tb(H_2O)(BTB)]$	turn-off fluorescence	0.035 μM	S3
$[Tb_{0.2}Y_{0.8}(FDA)(OX)_{0.5}(H_2O)_2]\cdot H_2O$	turn-off fluorescence	0.0022 μM	S4
UiO-66-NH_2 (pyrene-tagged)	turn-on and blue-shift fluorescence	73 μM	S5
Zn-DMBI	turn-on fluorescence	1.3 μM	S6
JXUST-13	turn-on and blue-shift fluorescence	2.7 μM	S7
JXUST-32	turn-on and red-shift fluorescence	0.11 μM	**This work**

Table S5. Comparison of different MOF materials for detecting CO_3^{2-}.

Sensors	**Detection technique**	**Limit of detection (LOD)**	**Ref.**
IRMOF-10-Eu	ratiometric sensor	9.58 μM	S8
Phen-MDI-CA/malachite	ratiometric sensor	0.00086 μM	S9
$\{[Zn_2(\mu_3\text{-}OH)(cpta)(4,4'bipy)]\cdot H_2O\}_n$	ratiometric sensor	5.55 μM	S10
Eu/Pt-MOFs	ratiometric sensor	0.021 μM	S11
$[Eu_2(Hhpip)_2(OAc)_6]$	ratiometric sensor	7.8 μM	S12
$\{[Eu(HL)(H_2O)_3]\cdot H_2O\}_n$	turn-off fluorescence	1.0 μM	S13
$[\{[Eu(HBPTC)(H_2O)_2]\cdot 2DMF\}_n]$	turn-off fluorescence	1.0 μM	S14
$[Tb(ppda)(ox)_{0.5}(H_2O)_2]_n$	turn-off fluorescence	0.38 μM	S15
(E)-3-(4-methoxyphenyl)-4-[(4-nitrobenzylidene)-amino]-1*H*-1,2,4-triazole-5(4*H*)-thione	turn-on fluorescence	1.91 μM	S16
JXUST-32	turn-on and red-shifted fluorescence	0.12 μM	**This work**

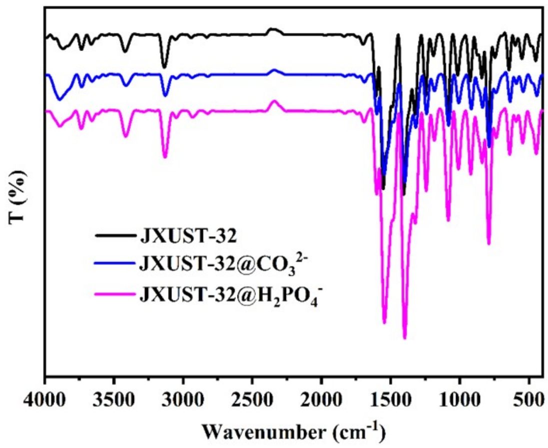

Fig. S1 IR spectra of **JXUST-32**, **JXUST-32**@$H_2PO_4^-$ and **JXUST-32**@CO_3^{2-} at room temperature.

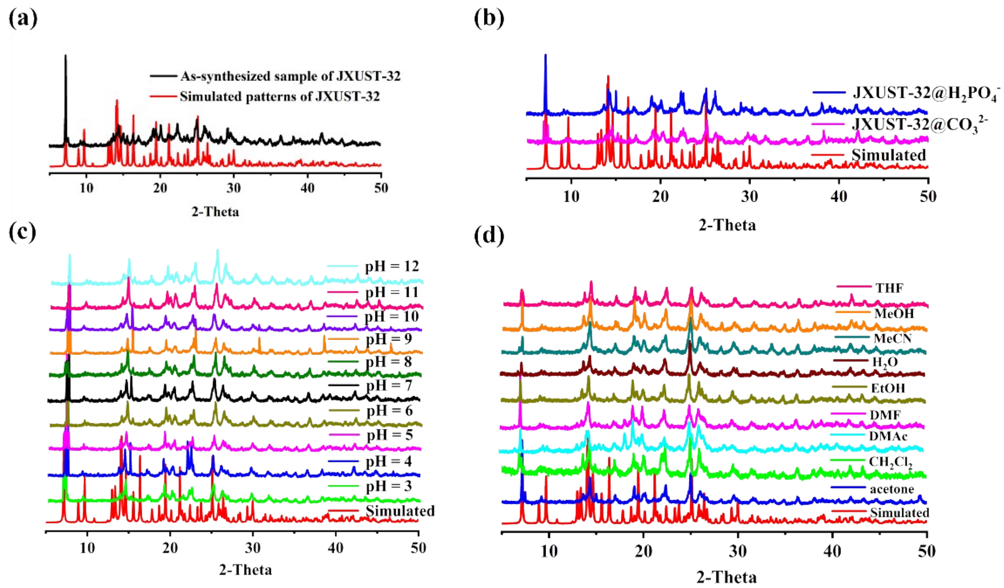

Fig. S2 (a) The simulated pattern for **JXUST-32** and the experimental patterns of the as-synthesized sample; (b) the simulated and experimental PXRD patterns of **JXUST-32** after sensing $H_2PO_4^-$and CO_3^{2-} for 5 cycles; (c) the simulated and experimental PXRD patterns of **JXUST-32** after immersing in common organic solvents for 24 hours; (d) the simulated and experimental PXRD patterns of **JXUST-32** immersed in aqueous solution with pH values of 2–12 for 24 hours.

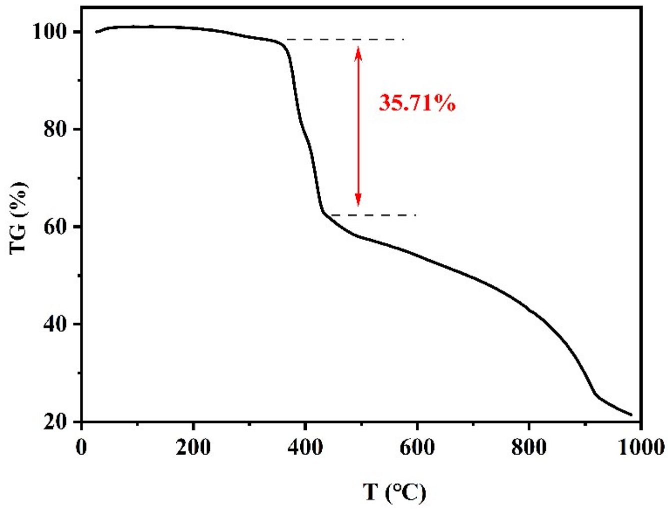

Fig. S3 The TGA curve of **JXUST-32** under N_2 atmosphere.

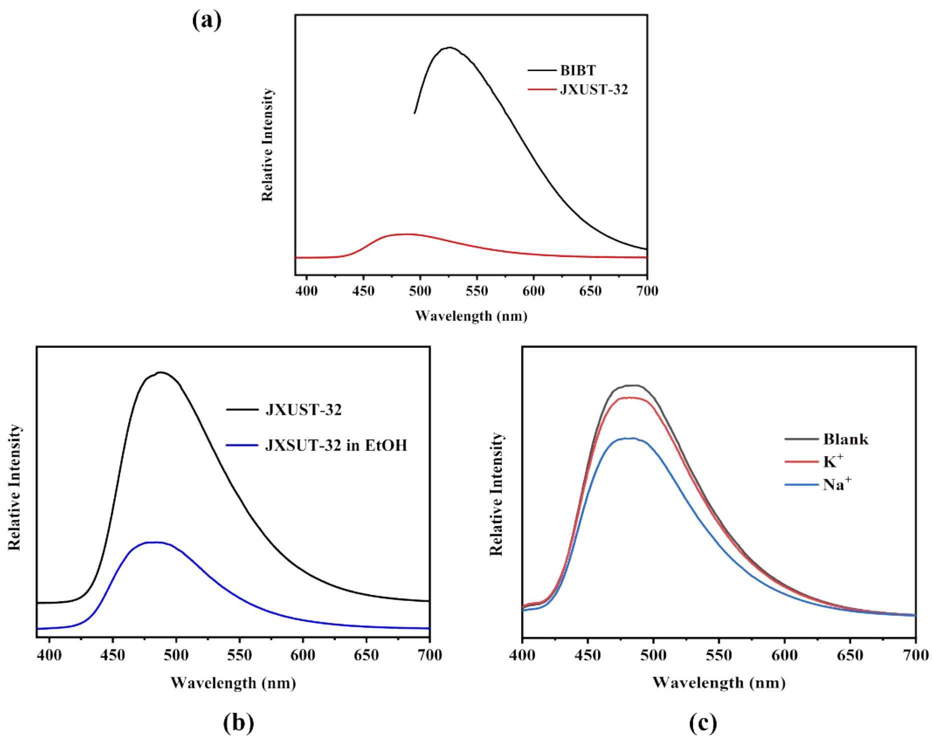

Fig. S4 (a) The solid-state emission spectra of BIBT and **JXUST-32**; (b) the emission spectra of **JXUST-32** and **JXUST-32** in EtOH solution at room temperature; (c) the emission spectra of **JXUST-32** upon the addition of K^+ and Na^+ ions in EtOH solution.

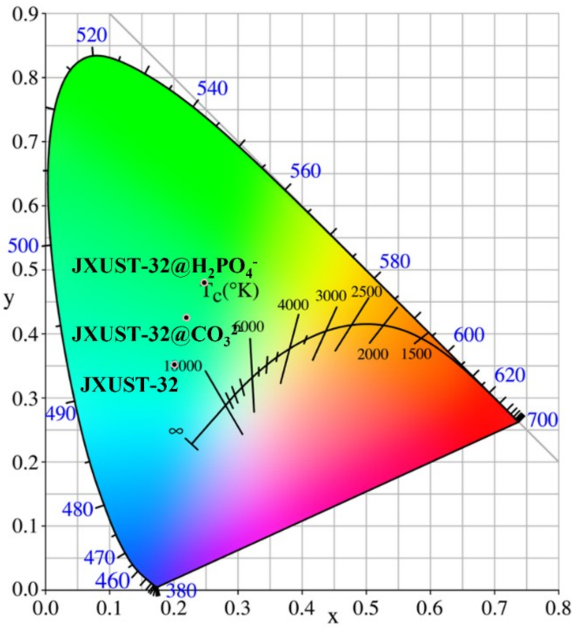

Fig. S5 CIE chromaticity diagram displaying the color coordinate of **JXUST-32**, **JXUST-32**@$H_2PO_4^-$ and **JXUST-32**@CO_3^{2-}.

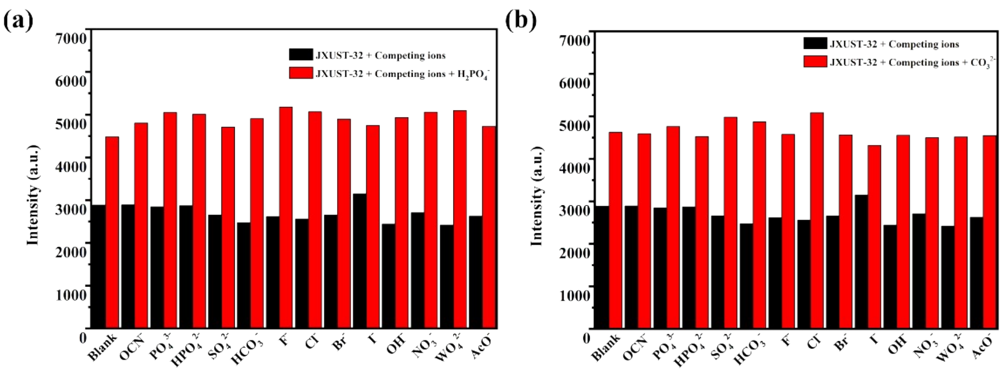

Fig. S6 The competition experiments of **JXUST-32** for the detection of (a) $H_2PO_4^-$ and (b) CO_3^{2-} interfered with other anions.

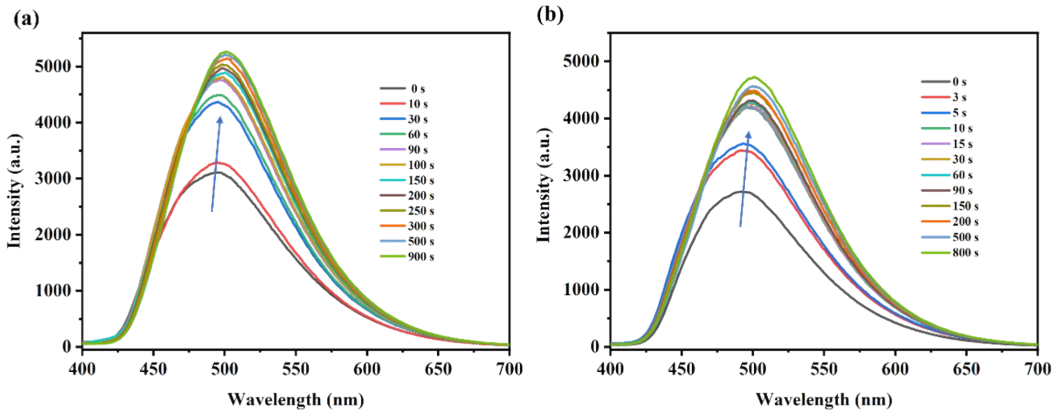

Fig. S7 Time-dependent emission spectra of the suspension after adding 0.2 mM (a) $H_2PO_4^-$ and (b) CO_3^{2-}, respectively.

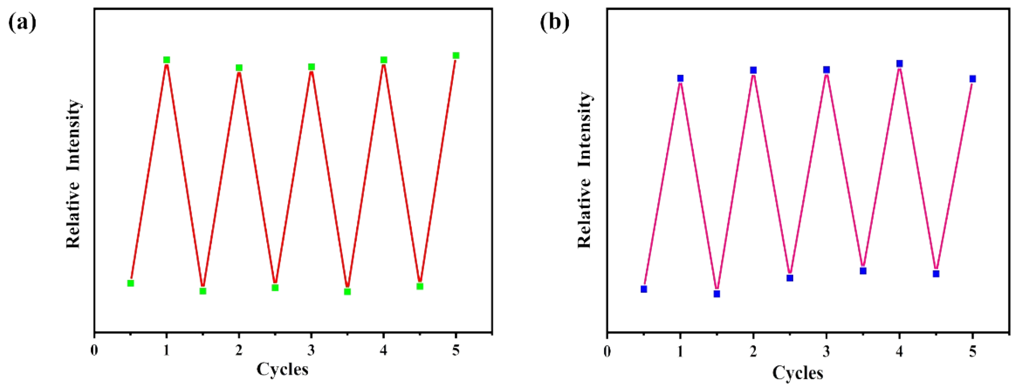

Fig. S8 Relative luminescent intensities of **JXUST-32** after five cycles for (a) $H_2PO_4^-$ ions and (b) CO_3^{2-} ions.

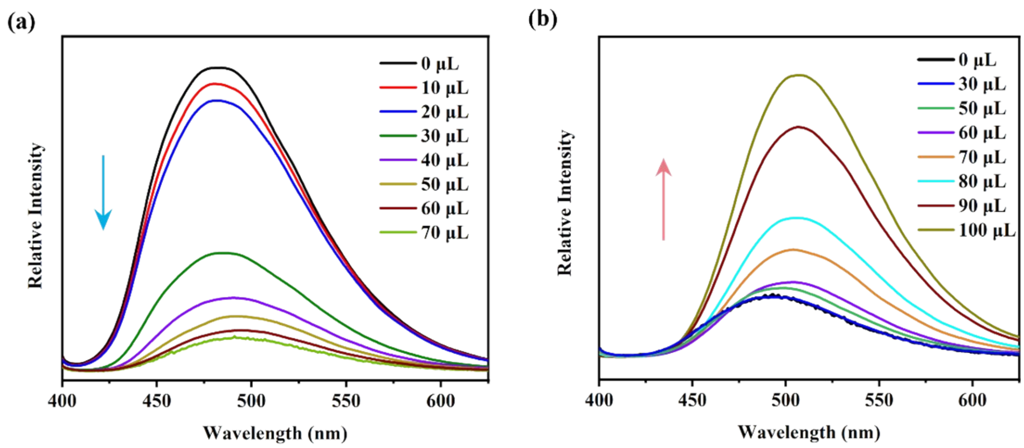

Fig. S9 (a) Photoluminescence intensity changes of **JXUST-32**@CO_3^{2-} upon the addition of HCl solution; (b) photoluminescence intensity changes of **JXUST-32**@CO_3^{2-} upon the addition of NaOH solution.

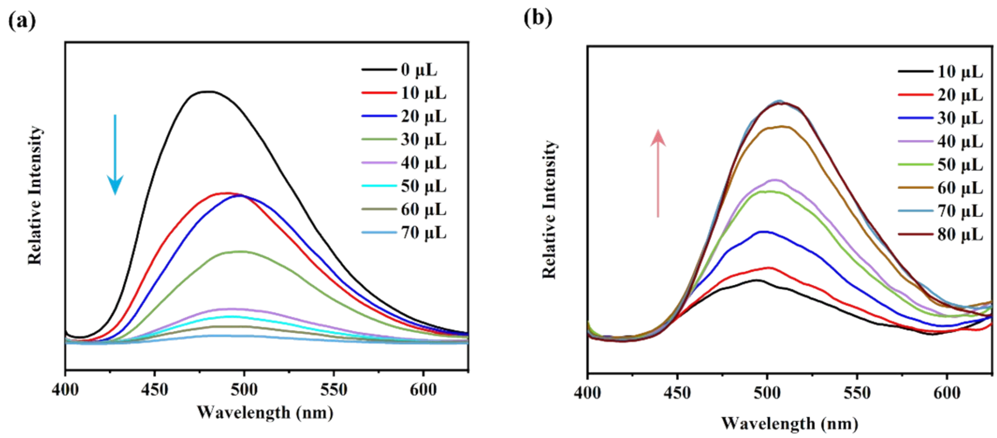

Fig. S10 (a) Photoluminescence intensity changes of **JXUST-32**@$H_2PO_4^-$ upon the addition of HCl solution; (b) photoluminescence intensity changes of **JXUST-32**@$H_2PO_4^-$ upon the addition of NaOH solution.

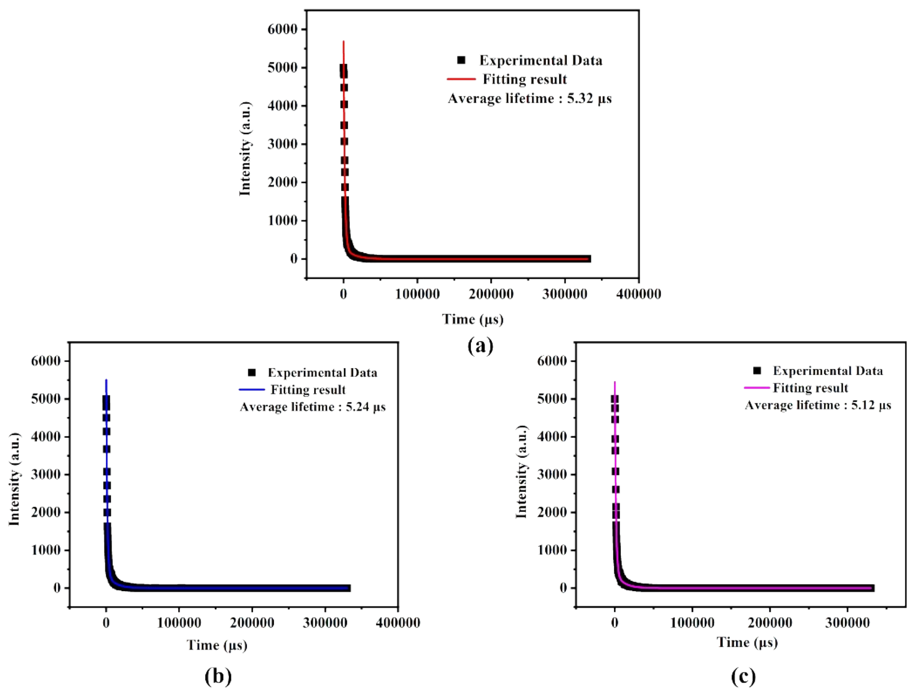

Fig. S11 The luminescence decay curves of (a) **JXUST-32**, (b) **JXUST-32**@CO_3^{2-} and (c) **JXUST-32**@$H_2PO_4^-$ at room temperature.

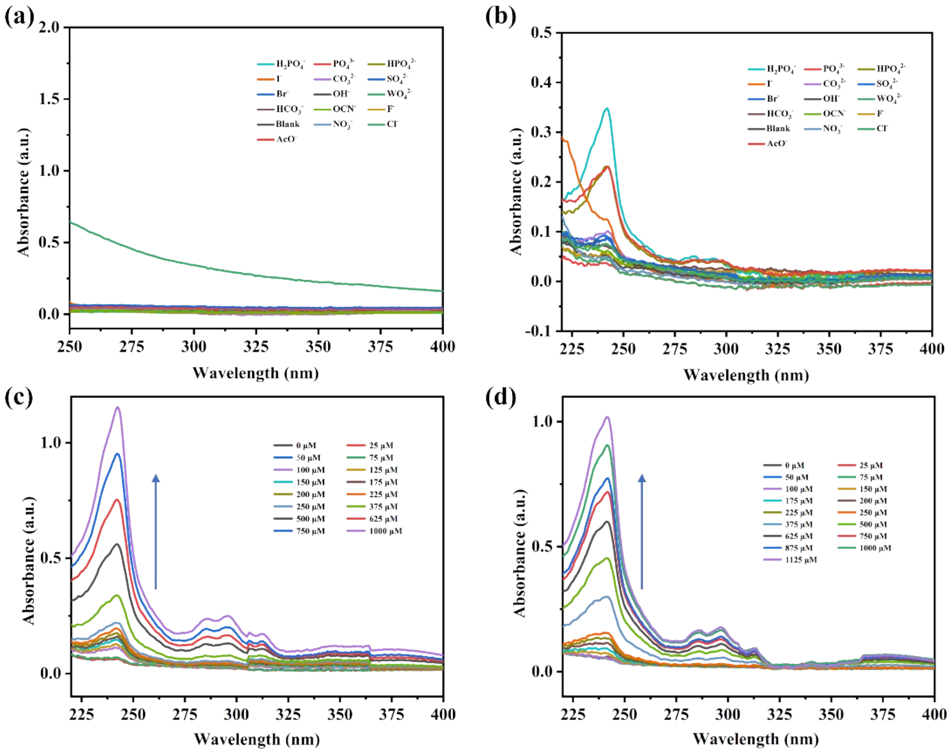

Fig. S12 (a) UV−vis absorbance spectra of various anions in EtOH solution; (b) UV−vis absorbance spectra of **JXUST-32** upon the addition of various anions; UV−vis absorbance spectra of **JXUST-32** dispersed in EtOH solution after adding different concentration of (c) $H_2PO_4^-$ and (d) CO_3^{2-}.

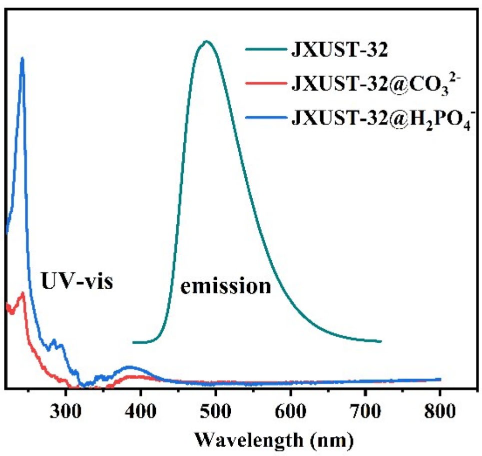

Fig. S13 The UV absorbance spectra of **JXUST-32**@$H_2PO_4^-$ and **JXUST-32**@CO_3^{2-}, and the emission spectrum of **JXUST-32**.

References

S1. X. M. Tian, S. L. Yao, J. Wu, H. Xie, T. F. Zheng, X. J. Jiang, Y. Wu, J. Mao and S. J. Liu, *Polyhedron*, 2019, **171**, 523-529.

S2. K. Naskar, A. K. Bhanja, S. Paul, K. Pal and C. Sinha, *Cryst. Growth Des.*, 2020, **20**, 6453-6460.

S3. K. S. Asha, R. Bhattacharjee and S. Mandal, *Angew. Chem. Int. Ed.,* 2016, **55**, 11528-11532.

S4. D. K. Singha, P. Majee, S. Hui, S. K. Mondal and P. Mahata, *Dalton Trans.*, 2020, **49**, 829-840.

S5. R. Dalapati and S. Biswas, *Sensor. Actuat. B-Chem.*, 2017, **239**, 759-767.

S6. S. Jindal and J. N. Moorthy, *Inorg. Chem.*, 2022, **61**, 3942-3950.

S7. S. Yao, H. Xu, T. Zheng, Y. Li, H. Huang, J. Wang, J. Chen, S. Liu and H. Wen, *Chin. Chem. Lett.*, 2023, **34**, 107532.

S8. Y. Wei and Y. Xia, *RSC Adv.*, 2020, **10**, 24764-24771.

S9. H. Nawaz, J. Zhang, W. Tian, K. Jin, R. Jia, T. Yang and J. Zhang, *J. Hazard. Mater.*, 2020, **387**, 121719.

S10. A. Ghorai, J. Mondal, R. Chandra and G. K. Patra, *RSC Adv.*, 2016, **6**, 72185-72192.

S11. N. N. Sun and B. Yan, *Dyes Pigm.*, 2017, **142**, 1-7.

S12. Y. N. Lu, J. L. Peng, X. Zhou, J. Z. Wu, Y. C. Ou and Y. P. Cai, *CrystEngComm*, 2018, **20**, 7574-7581.

S13. H. Wang, J. Qin, C. Huang, Y. Han, W. Xu and H. Hou, *Dalton Trans.*, 2016, **45**, 12710-12716.

S14. H. Liu, H. Wang, T. Chu, M. Yu and Y. Yang, *J. Mater. Chem. C*, 2014, **2**, 8683-8690.

S15. Z. Zhan, Y. Jia, D. Li, X. Zhang and M. Hu, *Dalton Trans.*, 2019, **48**, 15255-15262.

S16. Y. Wei and Y. Xia, *RSC Adv.*, 2020, **10**, 24764-24771.